

Tibial Tunnel Placement in ACL Reconstruction Using a Novel Grid and Biplanar Stereoradiographic Imaging

Julien Montreuil,^{*†‡} MD, MSc, Joseph Saleh,[§] Thierry Cresson,[†] PhD, Jacques A. De Guise,[†] PhD, and Frédéric Lavoie,^{||} MD, MSc

Investigation performed at Centre Hospitalier de l'Université de Montréal, Montréal, Québec, Canada

Background: Nonanatomic graft placement is a frequent cause of anterior cruciate ligament reconstruction (ACLR) failure, and it can be attributed to either tibial or femoral tunnel malposition. To describe tibial tunnel placement in ACLR, we used EOS, a low-dose biplanar stereoradiographic imaging modality, to create a comprehensive grid that combines anteroposterior (AP) and mediolateral (ML) coordinates.

Purpose: To (1) validate the automated grid generated from EOS imaging and (2) compare the results with optimal tibial tunnel placement.

Study Design: Descriptive laboratory study.

Methods: Using EOS, 3-dimensional models were created of the knees of 37 patients who had undergone ACLR. From the most medial, lateral, anterior, and posterior points on the tibial plateau of the EOS 3-dimensional model for each patient, an automated and personalized grid was generated from 2 independent observers' series of reconstructions. To validate this grid, each observer also manually measured the ML and AP distances, the medial proximal tibial angle (MPTA), and the tibial slope for each patient. The ideal tibial tunnel placement, as described in the literature, was compared with the actual tibial tunnel grid coordinates of each patient.

Results: The automated grid metrics for observer 1 gave a mean (95% CI) AP depth of 54.7 mm (53.4-55.9), ML width of 75.0 mm (73.3-76.6), MPTA of 84.9° (83.7-86.0), and slope of 7.2° (5.4-9.0). The differences with corresponding manual measurements were means (95% CIs) of 2.4 mm (1.4-3.4 mm), 0.5 mm (-1.3 to 2.2 mm), 1.2° (-0.4° to 2.9°), and -0.4° (-2.1° to 1.2°), respectively. The correlation between automated and manual measurements was $r = 0.78$ for the AP depth, $r = 0.68$ for the ML width, $r = 0.18$ for the MPTA, and $r = 0.44$ for the slope. The center of the actual tibial aperture on the plateau was a mean of 5.5 mm (95% CI, 4.8-6.1 mm) away from the referenced anatomic position, with a tendency toward more medial placement.

Conclusion: The automated grid created using biplanar stereoradiographic imaging provided a novel, precise, and reproducible description of the tibial tunnel placement in ACLR.

Clinical Relevance: This technique can be used during preoperative planning, intraoperative guidance, and postoperative evaluation of tibial tunnel placement in ACLR.

Keywords: knee; ACL; tridimensional modeling; stereoradiographic imaging; biomechanics of ligament; imaging and radiology

The anterior cruciate ligament (ACL) is an important stabilizer of the knee that is frequently injured. Globally, 400,000 ACL reconstructions (ACLRs) are performed each year.³⁰ Tibial and femoral tunnel malposition are a common cause of ACLR failure.³⁴ Although there are an abundance of studies describing the ideal femoral tunnel placement, there is much less of a focus in the literature on defining the optimal tibial tunnel positioning.³² Multiple reconstruction

techniques target an anatomic placement of the tibial and femoral tunnels.^{3,6,19,23,25,31,34,35} Tibial tunnels placed too far anteriorly may lead to increased graft obliquity and subsequent impingement, whereas grafts placed too far posteriorly may lead to increased anterior translational laxity.^{2,3,6,12,20,28} Several studies have used 3-dimensional (3D) computed tomography (CT) scans to examine anatomic landmarks and to guide intraoperative tibial tunnel placement.^{31,32,35} Other studies have focused on image-guided techniques, such as radiographs and CT scans, to evaluate tunnel placement on the tibial and femoral surfaces.³⁴ As the tibial plateau can be viewed as a 2-dimensional surface

The Orthopaedic Journal of Sports Medicine, 9(3), 2325967121989369
DOI: 10.1177/2325967121989369
© The Author(s) 2021

This open-access article is published and distributed under the Creative Commons Attribution - NonCommercial - No Derivatives License (<https://creativecommons.org/licenses/by-nc-nd/4.0/>), which permits the noncommercial use, distribution, and reproduction of the article in any medium, provided the original author and source are credited. You may not alter, transform, or build upon this article without the permission of the Author(s). For article reuse guidelines, please visit SAGE's website at <http://www.sagepub.com/journals-permissions>.



Figure 1. Three-dimensional models issued from the EOS imaging system. Image used with permission from EOS imaging.

in the axial plane, a grid could be used to describe the desired tunnel placement with 2 coordinates. For the anteroposterior (AP) direction, Amis and Jakob² were the original authors to popularize the placement as a percentage along a line of reference extending from the anterior portion of the proximal tibia to the most posterior portion, while being parallel to the tibial plateau.^{6,8,12,34} Other methods have considered the tibial slope and used the tibial articular surface to describe a given position with a percentage along the AP depth.⁶ For the mediolateral (ML) placement on an AP radiograph, few studies have described the optimal location of tunnel placement.^{20,27,34}

EOS is a biplanar stereoradiographic imaging modality (Figure 1) (EOS imaging, Paris, France). By capturing simultaneous radiographic images in AP and lateral views, the EOS system is able to generate 3D surface reconstructions. Capturing the images in an upright, load-bearing

position allows EOS to generate a true 1:1 scaled image with respect to length. In addition, EOS technology generates these images at a 10 times lower radiation level when compared with conventional films.^{13,14} A previous study by our group demonstrated that, compared with 3D CT scan, EOS 3D reconstruction is a precise and efficient technique with good inter- and intraobserver reproducibility.²²

In this study, we used the EOS imaging system to describe the tibial tunnel aperture location in ACLR using an automated grid reference of the tibial plateau. We expected the automated grid to correspond to manual measurements for direction (AP and ML) and angulation (medial proximal tibial angle [MPTA] and tibial slope in the sagittal plane).^{1,10,15,25} We also expected the actual postoperative tibial tunnel aperture position to be within proximity of the ideal tunnel location, described in the literature at 40% in the AP axis and 51% in the ML axis from the medial origin.^{6,9,20}

*Address correspondence to Julien Montreuil, MD, MSc, Laboratoire de recherche en Imagerie et Orthopédie de l'ETS du Centre de Recherche du Centre Hospitalier de l'Université de Montréal, 900 St Denis Street, Montreal, QC, Canada H2X 0A9 (email: julien.montreuil@mail.mcgill.ca).

[†]Laboratoire de recherche en Imagerie et Orthopédie de l'ETS, Montréal, Québec, Canada.

[‡]McGill Division of Orthopaedic Surgery, Montreal General Hospital, Montréal, Québec, Canada.

[§]Faculté de Médecine, Université de Sherbrooke, Sherbrooke, Québec, Canada.

^{||}Service de chirurgie orthopédique, Centre Hospitalier de l'Université de Montréal, Montréal, Québec, Canada.

Final revision submitted September 13, 2020; accepted October 16, 2020.

One or more of the authors has declared the following potential conflict of interest or source of funding: Sponsorship for this study was received from the Natural Sciences and Engineering Research Council of Canada, Canada Research Chairs, Mitacs, and MEDTEQ. T.C. and J.A.D.G. have received research support and royalties and have patents licensed to EOS Imaging. AOSSM checks author disclosures against the Open Payments Database (OPD). AOSSM has not conducted an independent investigation on the OPD and disclaims any liability or responsibility relating thereto.

Ethical approval for this study was obtained from the Centre Hospitalier de l'Université de Montréal (2008-2564, ND 07.059).

METHODS

Study Patients

After receiving ethics committee approval, we selected 37 study patients from the cohort “Prospective Collection of



Figure 2. Example of a 3-dimensional model reconstructed using the EOS system.

Clinical and Radiological Data in Knee Patients” at our institution in Montréal, Canada. The sample size included 25 men and 12 women with a mean \pm SD age of 31.8 ± 3.0 years; there were 21 right knees and 16 left knees. All patients had undergone ACLR by the same surgeon (F.L.), between 2008 and 2011, using a single-bundle technique using a hamstring autograft, constant graft sizing method, and a tibial guide set between 50° and 60° according to the patient’s anatomy. The medial half of the tibial eminence and the anterior horn of the lateral meniscus were important landmarks used. All patients were judged as having successful reconstructions and underwent post-operative EOS imaging of their lower limbs 6 months after surgery.

3D Models Issued From EOS Images

The 3D models were generated using a pair of EOS images with orthogonal oblique views, (Figure 2); this method facilitated the identification of anatomic landmarks for each patient because it limited the superposition of structures. The images were processed using IdefX software (Laboratoire de recherche en Imagerie et Orthopédie de l’ETS), and 3D reconstructions were generated for both the tibia and the femur of each knee in the study. The process of 3D reconstruction consisted of adjusting, for each bone, the position and the shape of a generic 3D model to the stereoradiographic images of each study patient. A moving least squares optimization technique allowed us to achieve fast detail-preserving deformation to find the best alignment between the 2 projected silhouettes of the 3D template model and the boundaries of the patient’s bones. The reconstructions benefited from an integrated reference system (Figure 3). Tibial tunnels were also identified on postoperative 3D reconstructions with the “conical shape” tool in IdefX. With this tool, the tibial aperture is defined as a circle around a central axis. Each 3D model was reconstructed separately by 2 independent observers (observer

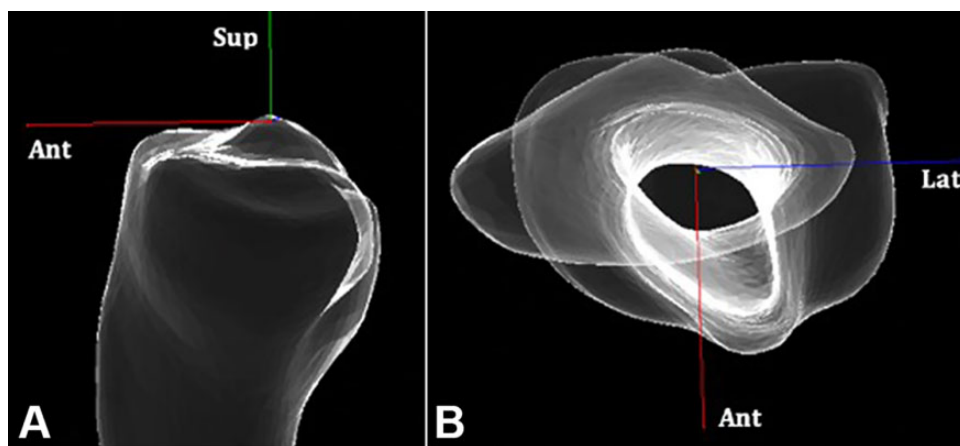


Figure 3. Generic reference system with 3-dimensional reconstructions of the proximal tibia before tibial tunnel segmentation. (A) Sagittal view. (B) Axial view of tibia. Ant, anterior; Lat, lateral; Sup, superior.

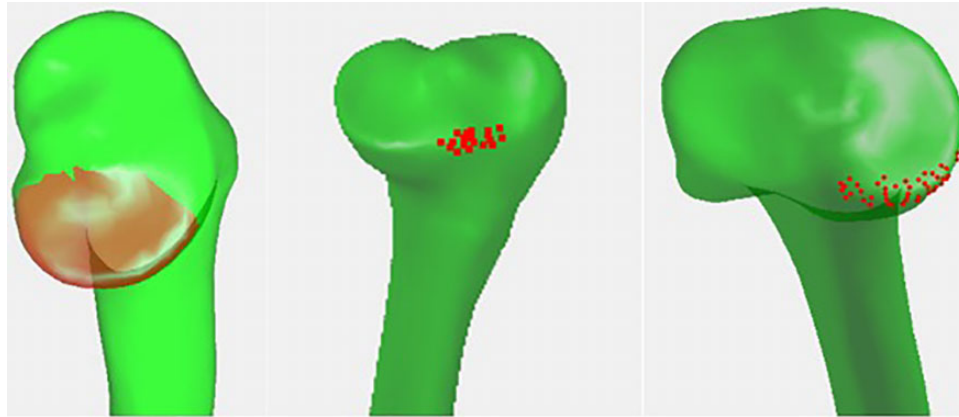


Figure 4. Automated region segmentation (red) from an EOS 3-dimensional model with medial (left image), anterior (middle), and posterior (right) points.

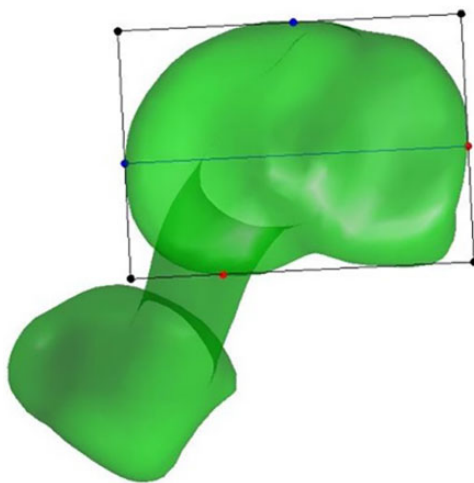


Figure 5. Automated grid delimitation.

1, J.M.; observer 2, J.S.) in order to test interobserver reliability.

Tibial Grid Conception

A rectangular grid was developed for each patient to describe the tunnel placement on the tibial plateau. Each of the 3D models issued from EOS had different regions mapped, which were used to automatically identify the most anterior, posterior, medial, and lateral points (Figure 4). A sagittal plane bisecting the plateau was defined and used to calculate the most medial and lateral points. The same technique with a coronal plane was used to identify the most anterior and posterior points. We defined the automated grid using 2 lines: 1 that extended from the medial and lateral points and 1, perpendicular, that extended from the anterior point to the posterior point. This grid then allowed us to describe any point on the tibial plateau as a percentage of the AP axis along with a percentage of the ML axis (Figure 5).

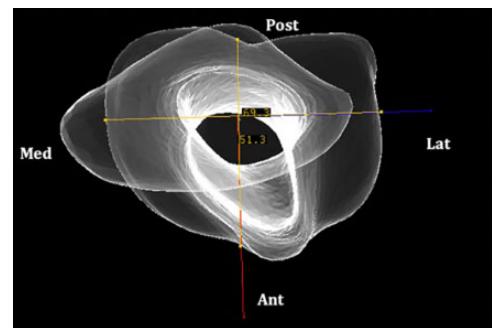


Figure 6. For automated grid validation, manual measurements of the anteroposterior depth and mediolateral width were obtained from 3-dimensional reconstructions for grid validation. Ant, anterior; Lat, lateral; Med, medial; Post, posterior.

Grid Validation

To validate our automated technique, the 2 observers manually measured 4 parameters on the 3D models: the AP depth, ML width, MPTA, and sagittal tibial slope. In order to obtain the manual measurements, the appropriate participant 3D reconstruction mesh was rotated to obtain optimal views. First, the AP depth and the ML width of the tibial plateau were measured on an axial view (Figure 6). Second, the tibial slope was measured on a sagittal view. Third, the MPTA was measured on the coronal view (Figure 7). The values obtained by each observer were compared with the automated values that were generated.

Anatomic Tunnel Placement

Using our 2-dimensional grid referential, we were able to define any point along the tibial plateau. The AP and ML coordinates were converted to percentages from the most anterior and lateral points, respectively. As described in the literature, the anatomic location of the ACL insertion on the tibial plateau was placed as 40% in the AP axis and

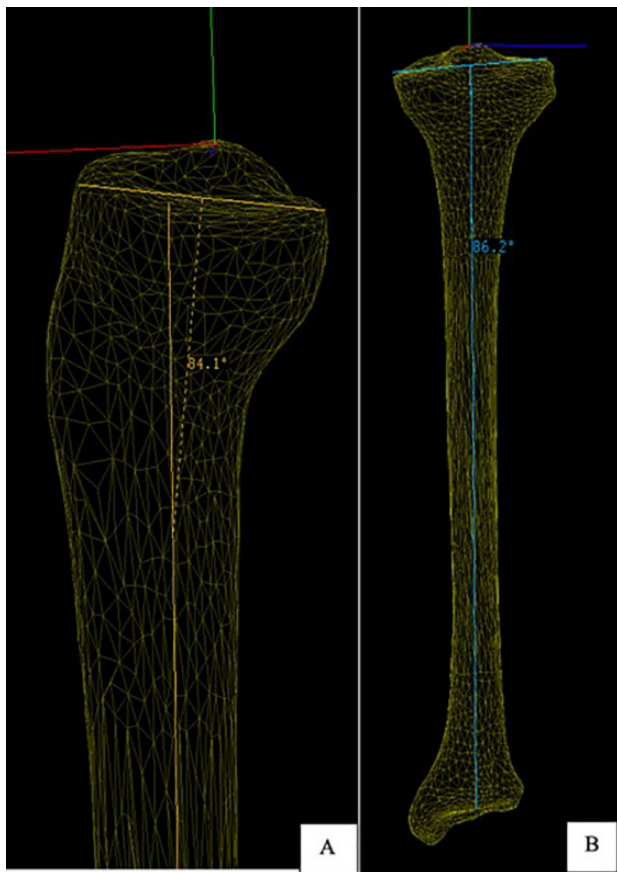


Figure 7. Manual measurements of (A) tibial slope and (B) medial proximal tibial angle for grid validation.

51% in the ML axis.^{6,9,20} With this anatomic position, we were able to compare the actual tibial tunnels in our models to the ideal operating point. For this project, the central axis of a best-fit circle in the tibial aperture was used. We calculated the Euclidean distance, which is a linear distance connecting the ideal point to the actual tibial tunnel aperture, for each patient.

Statistical Analysis

A minimum sample size of 25 patients for this study was calculated with an alpha of 5%, a power of 90%, an acceptable intraclass correlation coefficient (ICC) of 0.70, and an expected ICC of 0.90.⁵ Based on previous studies, the clinically important differences were set for length (3 mm) and angulation (4°).^{1,10,15,25} Estimates for ICCs and their 95% CIs were calculated using GraphPad Prism Version 8. The same software was used to perform paired Student *t* tests and Pearson correlation for the intertest correlation and the interobserver reliability study for all parameters. Reliability was determined as follows: ICC <0.5 indicated poor reliability, 0.5 to 0.74 indicated moderate reliability, 0.75 to 0.9 indicated good reliability, and >0.90 indicated excellent reliability.^{17,33}

TABLE 1
Tibial Grid Parameters From the 3-Dimensional Reconstructions of the Study Knees (N = 37)^a

	Observer 1		Observer 2	
	Mean	95% CI	Mean	95% CI
AP depth, mm				
Automated	54.7	53.4-55.9	53.9	52.6-55.2
Manual	52.3	50.8-53.8	52.1	50.5-53.7
ML width, mm				
Automated	75.0	73.3-76.6	73.7	72.2-75.1
Manual	75.4	73.1-77.7	72.1	70.1-74.2
Tibial slope, deg				
Automated	7.2	5.4-9.0	7.8	5.8-9.9
Manual	6.7	5.9-7.6	6.8	6.0-7.6
MPTA, deg				
Automated	84.9	83.7-86.0	84.9	83.7-86.2
Manual	86.1	85.2-87.0	86.5	85.7-87.4

^aAP, anteroposterior; ML, mediolateral; MPTA, medial proximal tibial angle.

RESULTS

The results of the EOS automated and manual measurements for the AP depth, ML width, MPTA, and sagittal tibial slope are shown in Table 1 and Figure 8. The grid metrics obtained from the automated method for observer 1 indicated a mean AP depth of 54.7 mm, ML width of 75.0 mm, tibial slope of 7.2°, and MPTA of 84.9°. The corresponding metrics measured manually were 52.3 mm, 75.4 mm, 6.7°, and 86.1°, respectively. The automated measures for observer 2 were 53.9 mm, 73.7 mm, 7.8°, and 84.9°, respectively. The corresponding manual metrics for observer 2 were 52.1 mm, 72.1 mm, 6.8°, and 86.5°, respectively (Figure 8). Differences between measuring modalities for all four tibial grid parameters are shown in Table 2.

Compared with the ideal anatomic position of the ACL, which is 40% in AP depth and 51% in ML width, the 3D reconstructions of observer 1 showed a mean tunnel position of 40.2% of AP depth and 54.3% of ML width (Table 3). The same metrics for the corresponding series of observer 2 were 41.4% for AP depth and 55.0% for ML width. For both observers, the mean Euclidean distance to the ideal position was 5.5 mm (Figure 9).

DISCUSSION

The purpose of this study was to describe the tibial tunnel aperture in ACLR using a novel grid reference from a 3D reconstruction of the proximal tibia, which was issued from an EOS biplanar imaging system. This grid, created using orthogonal lines through the most anterior, posterior, medial, and lateral positions of the tibial plateau, allows for the description of any desired point on the plateau. In order to validate this grid, the AP depth, ML width, MPTA, and sagittal slope were calculated both automatically and manually by 2 independent observers' series of 3D

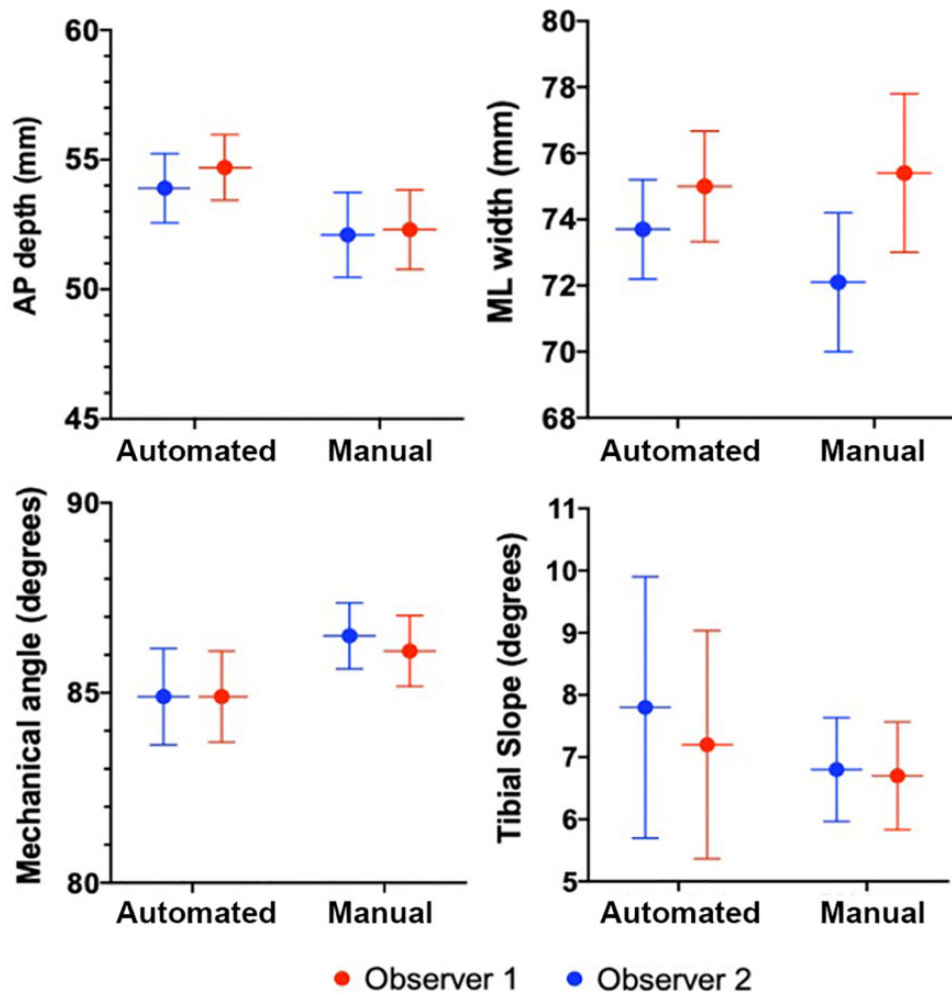


Figure 8. Validation of EOS automated grid parameters. AP, anteroposterior; ML, mediolateral.

reconstructions. The actual tibial apertures, identified by each observer during the reconstructions, were compared with the anatomic placement as described in the literature. Previous studies have developed and tested coordinate systems of the tibia using CT scans in order to automatically produce 3D reconstructions.^{16,21} Outlines using cross-sectional images created an ellipse on the tibial plateau with axes in both the AP and the ML directions.^{1,16} To the best of our knowledge, there have been no studies that have evaluated an automatic grid reference using the EOS imaging system. As previously stated, this biplanar stereoradiographic system has the ability to create 3D reconstructions in a true 1:1 scale for sizes, lengths, and angles while also emitting significantly less radiation.¹⁴

The 4 parameters chosen to validate our grid referential allowed us to conduct intertest analysis and interobserver reproducibility studies and interpret the results using equivalence tests. Dimensions and alignment of the tibial plateau are known from numerous previously conducted studies and helped establish equivalence thresholds. Cadaveric studies have shown that the mean dimensions were 50.5 ± 6.2 mm and 77.7 ± 5.9 mm for AP

depth and ML width of the tibial plateau, respectively.⁸ Imaging studies using CT scans have shown similar results, with 54.4 ± 5.2 mm and 74.4 ± 5.5 mm for AP depth and ML width, respectively.¹⁰ With respect to the tibial slope, it has been described to be 7° to 10° , with variability of 4.8° using planar imaging.^{1,4} Finally, for the MPTA, $87.2^\circ \pm 2.1^\circ$ is the value described in the literature.²⁴

In our study, when comparing both the manual and automated methods for the different parameters, the ML width and both coronal (MPTA) and sagittal (slope) angulation all showed no statistical difference while respecting our pre-established equivalence threshold. These results underline the overall validity of our automated method. Despite displaying a good correlation, the automated AP depth showed a significant difference compared with manual measurements and slightly surpassed the equivalence threshold of 3 mm. Because of the limited programmed handles to adjust the generic models, we believe that the posterior aspect of the plateau is the source of the discrepancies, especially at the posterolateral corner of the plateau. In fact, some reconstructions displayed a nonanatomic

TABLE 2
Intertest and Interobserver Analysis of Tibial Grid Parameters^a

	Paired <i>t</i> Test			Pearson Correlation	
	Difference	95% CI	<i>P</i>	<i>r</i>	<i>P</i>
AP depth, mm					
Automated ₁ vs manual ₁	2.4 ^b	1.4 to 3.4	<.0001	0.78	<.0001 ^c
Automated ₁ vs automated ₂	0.8 ^b	0.04 to 1.6	<.0001	0.81	<.0001 ^c
Manual ₁ vs manual ₂	0.2 ^b	-0.8 to 1.2	.73	0.81	<.0001 ^c
ML width, mm					
Automated ₁ vs manual ₁	0.5 ^b	-1.3 to 2.2	.60	0.68	<.0001 ^c
Automated ₁ vs automated ₂	1.3 ^b	0.5 to 2.1	.004	0.87	<.0001 ^c
Manual ₁ vs manual ₂	3.3	1.1 to 5.5	.005	0.53	.004 ^c
MPTA, deg					
Automated ₁ vs manual ₁	1.2 ^b	-0.4 to 2.9	.14	0.18	.14
Automated ₁ vs automated ₂	-0.1 ^b	-1.0 to 0.9	.87	0.70	<.0001 ^c
Manual ₁ vs manual ₂	-0.5 ^b	-1.3 to 0.4	.28	0.53	.0003 ^c
Tibial slope, deg					
Automated ₁ vs manual ₁	-0.4 ^b	-2.1 to 1.2	.60	0.44	.003 ^c
Automated ₁ vs automated ₂	-0.7 ^b	-3.2 to 1.8	.60	0.20	.12
Manual ₁ vs manual ₂	-0.1 ^b	-0.9 to 0.8	.91	0.54	.0003 ^c

^aSubscript numbers indicate observer number. AP, anteroposterior; ML, mediolateral; MPTA, medial proximal tibial angle.

^bWithin clinically important difference for that variable. Thresholds are stated in the Methods section.^{1,10,15,25}

^cStatistically significant (*P* < .05).

prominence. In order to limit outliers, we excluded this posterolateral surface when searching for the most posterior point. A suboptimal definition of the posterior point could therefore explain the variabilities seen on the AP depth and sagittal angulation measures (slope). For the MPTA, although there was only a 1.2° mean difference between both the automated and manual measurements, the correlation between both modalities was the weakest. We believe this can most likely be attributed to the imprecision in the manual measurements compared with the automated technique, which used fixed points in defining the MPTA. This observation is supported by an overall interobserver reproducibility that was superior in the automated method compared with manual measures.

In fact, by having both manual and automated measures for both observers, we were able to compare the interobserver reproducibility of the automated technique to that of the manual technique. With respect to the AP depth, both the automated and the manual measures were equivalent,

TABLE 3
Tibial Tunnel Aperture Position^a

	AP Ratio, %		ML Ratio, %		Δ to Anatomic Position, mm	
	Mean	95% CI	Mean	95% CI	Mean	95% CI
Observer 1	40.2	37.9-42.6	54.3	53.2-55.4	5.5	4.8-6.1
Observer 2	41.4	39.4-43.3	55.0	54.2-55.9	5.5	4.8-6.1
ICC	0.57 (<i>P</i> = .0002 ^b)		0.52 (<i>P</i> = .009 ^b)		0.49 (<i>P</i> = .002 ^b)	

^aIdeal anteroposterior (AP) ratio = 40%, ideal mediolateral (ML) ratio = 51%. ICC, intraclass correlation coefficient.

^bStatistically significant (*P* < .05).

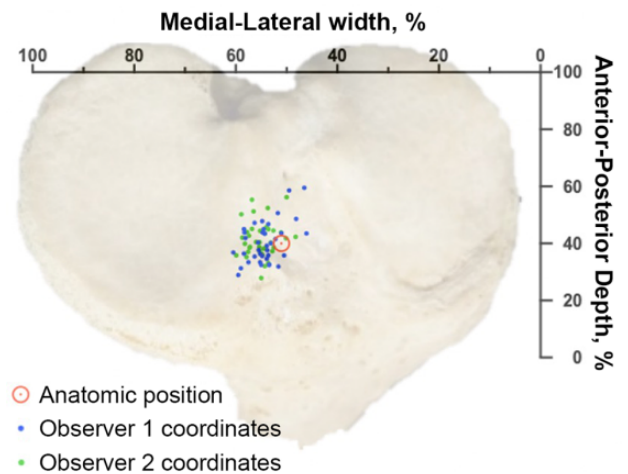


Figure 9. Actual tibial tunnel position and coordinates from observers 1 and 2.

displaying good correlation (*r* = 0.81; *P* < .0001). Most importantly, to highlight the advantage of the automated process, for the ML width and MPTA, the automated technique displayed greater reproducibility than did the manual technique. The automated measures displayed good correlation for both ML width and MPTA (*r* = 0.87, *P* < .0001; and *r* = 0.70, *P* < .0001, respectively), whereas the manual technique displayed moderate correlation for both ML width and MPTA (*r* = 0.53, *P* = .0003; and *r* = 0.54, *P* = 0.003, respectively).

The final objective of this study was to describe the mean Euclidean distance between the optimal tunnel position and the actual apertures identified on our models (Figure 9). We used percentages along the AP depth and ML width of the tibial plateau as coordinates. With respect to the cited anatomic points of 40% in the AP direction and 51% in the ML direction, the mean Euclidean distance was measured with both observers obtaining 5.5 mm (95% CI, 4.8-6.1),^{6,9,20} erring more medially. These results are comparable with techniques using magnetic resonance imaging for tibial tunnel positioning analysis.²⁶ This precision on a surgical level is also satisfying when considering the large anatomic tibial footprints described in the literature.¹⁸ Edwards et al.¹¹ described the length of the footprint to

be 18 ± 2 mm and the width 9 ± 2 mm. Figure 9 illustrates the tendency toward a more anteromedial placement of the tibial tunnel. It places the posterolateral aspect of the tibial aperture overlying the ideal position. Therefore, because the graft sits in the posterolateral aspect of the tibial aperture, this may become the ideal biomechanical position.²⁹ This eccentric tunnel aperture placement was noted by Clancy et al.⁷ Biomechanical and clinical effects of such small differences have yet to be shown. Overall, this automated grid technique adequately described both the AP depth and ML width coordinates of drilled tibial tunnels in an ACLR.

Combining this tibial grid with the femoral reference system described by our group could offer numerous possibilities. Further studies could evaluate the effect of preoperative planning and the precision of individualized surgical guides. Another avenue could be to overlay the 3D reconstructions and ideal targets on the actual arthroscopy screen. This tool could also be used for postoperative feedback in ACLR. We could compare tunnel placement between surgeons or different placement techniques. Finally, we aim to analyze clinical outcomes depending on tunnel position.

Although promising results were obtained using this novel grid reference, there are limitations to our study. As each model was 3D reconstructed semimanually by each observer, human operator imprecisions in the reconstructions may have affected the results. Indeed, having completely automated reconstructions would likely improve the accuracy and reliability of the reconstructions while speeding up an already efficient process. As discussed earlier, given the limited programmed handles to adjust the generic models, the most posterior point on the automated models was restricted to the posteromedial region because of posterolateral inaccuracies seen in the 3D reconstructions, which were excluded. A suboptimal definition of the posterior point could explain the variabilities seen on the AP depth and sagittal angulation (slope) measures. We suggest further refining of this posterolateral region on the 3D models in future studies.

Another improvement could be to integrate an oval shape as the intra-articular aperture. This would respect the actual aperture shape, its effect on graft placement, and considerations toward eccentric positioning. Moreover, our database consisted of patients who underwent ACLR by a single surgeon using a single technique. While this represents a limitation to our study with regard to its external validity, it allowed us to limit confounding factors and evaluate its reliability. We also want to emphasize the fact that the ideal location of tunnel drilling in ACLR has yet to be found through clinical and biomechanical studies. We are well aware that further studies could support different placement than the one shared in this paper.

Finally, the accessibility of such a system is limited, restricting our knowledge about reproducibility among different centers. This reproducibility will need to be established before our technique is scaled. Sharing data among institutions using EOS will augment the sample size while obtaining results from other surgeons with different

surgical techniques. This should improve the precision and generalizability of our method. Although it was not the aim of the present radiologic descriptive study, evaluating the clinical effect of the tunnel's position in ACLR remains a priority of our group.

CONCLUSION

This novel automated coordinate system using biplanar stereoradiographic low-irradiation imaging showed a precision comparable with that of standard manual measurements in ACLR tibial tunnel placement. Our results suggest that the automated grid issued from EOS knee reconstruction shows good accuracy and reproducibility. Although the results of this preliminary study are promising, we strive to improve our method by refining further parameters to evaluate and revalidate the present technique.

REFERENCES

1. Amirtharaj MJ, Hardy BM, Kent RN III, et al. Automated, accurate, and three-dimensional method for calculating sagittal slope of the tibial plateau. *J Biomech*. 2018;79:212-217.
2. Amis AA, Jakob RP. Anterior cruciate ligament graft positioning, tensioning and twisting. *Knee Surg Sports Traumatol Arthrosc*. 1998; 6(suppl 1):S2-S12.
3. Bedi A, Maak T, Musahl V, et al. Effect of tunnel position and graft size in single-bundle anterior cruciate ligament reconstruction: an evaluation of time-zero knee stability. *Arthroscopy*. 2011;27(11):1543-1551.
4. Bernhardson AS, Aman ZS, Dornan GJ, et al. Tibial slope and its effect on force in anterior cruciate ligament grafts: anterior cruciate ligament force increases linearly as posterior tibial slope increases. *Am J Sports Med*. 2019;47(2):296-302.
5. Bujang MA. A simplified guide to determination of sample size requirements for estimating the value of intraclass correlation coefficient: a review. *Arch Orofacial Sci*. 2017;12:1-11.
6. Cho HJ, Kim TK, Kang SB, Do MU, Chang CB. Variations in sagittal locations of anterior cruciate ligament tibial footprints and their association with radiographic landmarks: a human cadaveric study. *BMC Musculoskelet Disord*. 2017;18(1):448.
7. Clancy WG Jr, Nelson DA, Reider B, Narechania RG. Anterior cruciate ligament reconstruction using one-third of the patellar ligament, augmented by extra-articular tendon transfers. *J Bone Joint Surg Am*. 1982;64(3):352-359.
8. Colombet P, Robinson J, Christel P, et al. Morphology of anterior cruciate ligament attachments for anatomic reconstruction: a cadaveric dissection and radiographic study. *Arthroscopy*. 2006;22(9): 984-992.
9. de Abreu-e-Silva GM, de Oliveira MH, Maranhao GS, et al. Three-dimensional computed tomography evaluation of anterior cruciate ligament footprint for anatomic single-bundle reconstruction. *Knee Surg Sports Traumatol Arthrosc*. 2015;23(3):770-776.
10. Ducouret E, Loriaut P, Boyer P, et al. Tunnel positioning assessment after anterior cruciate ligament reconstruction at 12 months: comparison between 3D CT and 3D MRI. A pilot study. *Orthop Traumatol Surg Res*. 2017;103(6):937-942.
11. Edwards A, Bull AM, Amis AA. The attachments of the anteromedial and posterolateral fibre bundles of the anterior cruciate ligament: Part 1: tibial attachment. *Knee Surg Sports Traumatol Arthrosc*. 2007;15: 1414-1421.
12. Hatayama K, Terauchi M, Saito K, Higuchi H, Yanagisawa S, Takagishi K. The importance of tibial tunnel placement in anatomic double-bundle anterior cruciate ligament reconstruction. *Arthroscopy*. 2013; 29(6):1072-1078.

13. Hui SCN, Pialasse J-P, Wong JYH, et al. Radiation dose of digital radiography (DR) versus micro-dose x-ray (EOS) on patients with adolescent idiopathic scoliosis: 2016 SOSORT-IRSSD “John Sevastic Award” winner in imaging research. *Scoliosis Spinal Disord.* 2016; 11(1):46.
14. Illes T, Somoskeoy S. The EOS imaging system and its uses in daily orthopaedic practice. *Int Orthop.* 2012;36(7):1325-1331.
15. Johannsen AM, Cook AM, Gardner MJ, Bishop JA. Defining the width of the normal tibial plateau relative to the distal femur: critical normative data for identifying pathologic widening in tibial plateau fractures. *Clin Anat.* 2018;31(5):688-692.
16. Kai S, Sato T, Koga Y, et al. Automatic construction of an anatomical coordinate system for three-dimensional bone models of the lower extremities—pelvis, femur, and tibia. *J Biomech.* 2014;47(5):1229-1233.
17. Koo TK, Li MY. A guideline of selecting and reporting intraclass correlation coefficients for reliability research. *J Chiropr Med.* 2016;15(2):155-163.
18. Kopf S, Musahl V, Tashman S, Szczodry M, Shen W, Fu FH. A systematic review of the femoral origin and tibial insertion morphology of the ACL. *Knee Surg Sports Traumatol Arthrosc.* 2009;17(3):213-219.
19. Lee JK, Lee S, Seong SC, Lee MC. Anatomy of the anterior cruciate ligament insertion sites: comparison of plain radiography and three-dimensional computed tomographic imaging to anatomic dissection. *Knee Surg Sports Traumatol Arthrosc.* 2015;23(8):2297-2305.
20. Lintner DM, Dewitt SE, Moseley JB. Radiographic evaluation of native anterior cruciate ligament attachments and graft placement for reconstruction: a cadaveric study. *Am J Sports Med.* 1996;24(1):72-78.
21. Miranda DL, Rainbow MJ, Leventhal EL, Crisco JJ, Fleming BC. Automatic determination of anatomical coordinate systems for three-dimensional bone models of the isolated human knee. *J Biomech.* 2010;43(8):1623-1626.
22. Montreuil J, Saleh J, Cresson T, De Guise JA, Lavoie F. Femoral tunnel placement analysis in ACL reconstruction through use of a novel 3-dimensional reference with biplanar stereoradiographic imaging. *Orthop J Sports Med.* 2020;8(4):2325967120915709.
23. Nakamae A, Ochi M, Deie M, et al. Clinical outcomes of second-look arthroscopic evaluation after anterior cruciate ligament augmentation: comparison with single- and double-bundle reconstruction. *Bone Joint J.* 2014;96-B(10):1325-1332.
24. Paley D, Herzenberg JE. *Principles of Deformity Correction.* Springer Electronic Media; 2004.
25. Parkar AP, Adriaensen M, Giil LM, Solheim E. Computed tomography assessment of anatomic graft placement after ACL reconstruction: a comparative study of grid and angle measurements. *Orthop J Sports Med.* 2019;7(3):2325967119832594.
26. Pedneault C, Laverdiere C, Hart A, Boily M, Burman M, Martineau PA. Evaluating the accuracy of tibial tunnel placement after anatomic single-bundle anterior cruciate ligament reconstruction. *Am J Sports Med.* 2019;47(13):3187-3194.
27. Pietrini SD, Ziegler CG, Anderson CJ, et al. Radiographic landmarks for tunnel positioning in double-bundle ACL reconstructions. *Knee Surg Sports Traumatol Arthrosc.* 2011;19(5):792-800.
28. Pinczewski LA, Salmon LJ, Jackson WF, von Bormann RB, Haslam PG, Tashiro S. Radiological landmarks for placement of the tunnels in single-bundle reconstruction of the anterior cruciate ligament. *J Bone Joint Surg Br.* 2008;90(2):172-179.
29. Purnell ML, Larson AI, Clancy W. Anterior cruciate ligament insertions on the tibia and femur and their relationships to critical bony landmarks using high-resolution volume-rendering computed tomography. *Am J Sports Med.* 2008;36(11):2083-2090.
30. Rayan F, Nanjayan SK, Quah C, Ramoutar D, Konan S, Haddad FS. Review of evolution of tunnel position in anterior cruciate ligament reconstruction. *World J Orthop.* 2015;6(2):252-262.
31. Shimodaira H, Tensho K, Akaoka Y, Takanashi S, Kato H, Saito N. Remnant-preserving tibial tunnel positioning using anatomic landmarks in double-bundle anterior cruciate ligament reconstruction. *Arthroscopy.* 2016;32(9):1822-1830.
32. Shimodaira H, Tensho K, Akaoka Y, Takanashi S, Kato H, Saito N. Tibial tunnel positioning technique using bony/anatomical landmarks in anatomical anterior cruciate ligament reconstruction. *Arthrosc Tech.* 2017;6(1):e49-e55.
33. Shrout PE, Fleiss JL. Intraclass correlations: uses in assessing rater reliability. *Psychol Bull.* 1979;86(2):420-428.
34. Sullivan JP, Cook S, Gao Y, Wolf BR. Radiographic anatomy of the native anterior cruciate ligament: a systematic review. *HSS J.* 2015; 11(2):154-165.
35. Tensho K, Shimodaira H, Aoki T, et al. Bony landmarks of the anterior cruciate ligament tibial footprint: a detailed analysis comparing 3-dimensional computed tomography images to visual and histological evaluations. *Am J Sports Med.* 2014;42(6):1433-1440.